Ocean Engineering 266 (2022) 112840

Contents lists available at ScienceDirect

Ocean Engineering

journal homepage: www.elsevier.com/locate/oceaneng

Investigation of internal wave wakes generated by a submerged body in a stratified flow

Jin Chai [a,b], Zhiying Wang [a,*], Zixuan Yang [a,b], Zhan Wang [a,b,**]

[a] Institute of Mechanics, Chinese Academy of Sciences, Beijing, 100190, PR China
[b] School of Engineering Science, University of Chinese Academy of Sciences, Beijing, 100049, PR China

ARTICLE INFO

Keywords:
Stratified flow
Internal wave wakes
Large eddy simulation

ABSTRACT

Internal waves in the ocean with stratified structure are essential: natural internal waves for the untangling of physical and environmental processes in oceanography and internal waves generated by a submerged moving body for understanding the near-field flow structures and wave patterns for detection. The latter in a stratified flow with a pycnocline presented are investigated numerically in the present paper. Systematic analyses on the influences of different hydrodynamic parameters, including the Froude number (*Fr*), the Reynolds number (Re), the thickness of the pycnocline (Δ_L), and the relative position of the submerged body (Δ_d), on internal wave wakes, are performed. A variation trend diagram of wake angle and wave amplitude for different parameters is obtained, showing the order of influence: $Fr > \Delta_L > \Delta_d > \mathrm{Re}$. For two key parameters, *Fr* and Δ_L, scalings of wake angle variation are found. Wake angle shows a -1 power-law dependence on *Fr* and the same order power law on Δ_L in a critical range. In addition, vortex structures and turbulent kinetic energy distributions in the wakes are explored by comparing to the homogeneous case.

1. Introduction

Across the world's oceans, variation of density caused by thermohaline structure gives rise to density disturbances that can propagate in the form of internal waves. There has been growing interest in the effect of stratification on several essential processes in physical oceanography as well as geophysical, industrial, and environmental applications. For example, aiming to understand the global cascade of energy in ocean currents, numerical simulations and site experiments are performed to study natural internal solitary waves along with stratification and shear effects (Lamb and Warn-Varnas, 2015; Hartharn-Evans et al., 2022; Stastna et al., 2021; Prasetya et al., 2021). Researches associated with applications focus on the coupling dynamics between natural internal waves and offshore structures such as gas risers and oil risers (Ding et al., 2020; Ali et al., 2022; Guo et al., 2022). On the other side, internal waves generated by a source of disturbance, such as a submerged moving body or bottom topography, are also worth attention. Due to the presence of stratification, these internal waves often have a regular pattern and can last for several days, which provides a possibility for detection through synthetic aperture radar (SAR) and infrared (IR) detectors. The motivation for investigating these internal wave wakes is that understanding the bulk flow and turbulent wakes remains a hot topic and a challenging and significant task in ocean engineering. Corresponding researches can provide crucial information about the flow field features, design for the submerged body in terms of hydrodynamic parameters, and potential effective detection strategies.

Wakes generated by a moving source of disturbance exist commonly and widely (Meunier and Spedding, 2006). Experiments show that even a slight acceleration or change in the direction of the moving object can give rise to large-scale structures in the wake that decay in several days (Voropayev et al., 1999), which provides information and traces for detection. In the ocean environment, wakes are categorized into four regions: large-scale stationary free surface Kelvin waves, internal Kelvin-wave patterns (also called internal lee waves), small-scale non-stationary turbulent wakes, and wake-generated internal waves (Qiang et al., 1993).

The V-shaped free surface Kelvin waves on deep water generated by a moving body with a uniform velocity and always delimited by an angle of 19.47° were first proposed by Lord Kelvin (Dias, 2014). However, Rabaud and Moisy (2013, 2014) noticed that under large *Fr*, the Kelvin

* Corresponding author.
** Corresponding author. Institute of Mechanics, Chinese Academy of Sciences, Beijing, 100190, PR China.
E-mail addresses: wangzhiying@imech.ac.cn (Z. Wang), zwang@imech.ac.cn (Z. Wang).

https://doi.org/10.1016/j.oceaneng.2022.112840
Received 1 August 2022; Received in revised form 9 September 2022; Accepted 6 October 2022
Available online 17 October 2022

wake angle is not constant but reduces as Fr^{-1} with the increase of *Fr*. Darmon et al. (2014) performed a theoretical study and showed that the wake angle of the maximum wave amplitude has the same behavior as highlighted by Rabaud and Moisy. Based on theoretical analyses considering nonlinearity, Pethiyagoda et al. (2014, 2017) also observed a decrease in wake angle for sufficiently high *Fr*, and they pointed out that the nonlinearity significantly influences the wake angle.

In contrast to free surface Kelvin waves, the behavior of internal wave wakes is more complicated due to the influence of background stratification in the pycnocline. Keller and Munk (1970) solved the internal waves generated by a moving source in the pycnocline. They found that although a similar V-shaped Kelvin wave pattern exists, the cusps of wavefronts are located periodically along the streamwise direction, which is different from surface Kelvin waves. Gray et al. (1983) studied the case where a monopole or a dipole moves in the pycnocline, and a smooth Mach front was found at large distances behind the source in the linear approximation. Zhang et al. (2021) used the Euler equation and source-sink distribution method to numerically integrate the theoretical solutions of internal waves. They confirmed that the features of internal lee waves depend on the Froude number, and when it exceeds a critical value, the transverse waves disappear for the first mode (Zhang et al., 2021). Although internal lee waves have been investigated based on various theoretical methods (Keller et al., 1981; Borovikov et al., 1995; Yeung and Nguyen, 1999; Wei et al., 2003; Vasholz, 2011), it is found that the internal wave wakes are consist of the superposition of stationary internal lee waves and non-stationary waves generated by the turbulent structures (Bonneton et al., 1993; Spedding, 1997, 2014; Bonnier and Eiff, 2002; Abdilghanie and Diamessis, 2013; Meunier et al., 2018). At low *Fr*, internal lee waves are the dominant structures, while non-stationary waves gradually become dominant with the increase of *Fr*. Robey (1997) performed experiments on a towed sphere under various internal Froude numbers Fr_N ($Fr_N = U_0/Nd$, where N is the constant buoyancy frequency of uniform stratification, and U_0 and d are the moving velocity and diameter of the body, respectively) and indicated that the transition value of Fr_N from the stationary internal lee waves to the non-stationary waves is about $Fr_N = 2$. Brandt and Rottier (2015) also conducted a series of experiments, and their results showed that internal lee waves are the dominant mechanisms for $Fr_N \leqslant 1$. Wang et al. (2017) found that the transition value depends linearly on the submerged body aspect ratio. Due to technical challenges, experimental investigations of internal wave wakes are still limited.

With the development of computing capacity and numerical algorithms, numerical simulations are applied to capture more details of internal wave wakes. Ma et al. (2020) used the Reynolds Average Navier-Stokes (RANS) method to study the characteristics of internal waves. Huang et al. (2022) simulated the wake signatures of a submarine using RANS and indicated that stratification plays a role in the generation of wakes and their downstream evolution. The large-eddy simulation (LES) provides an appropriate way to capture small-scale structures to gain insight into the non-stationary internal waves. Chen et al. (2021) used the LES method and considered salinity and temperature variations. They marked similar distribution of Kelvin-wave patterns for disturbance fields whose values are in the detectable range. Zhou and Diamessis (2019) performed LES with a spectral method focusing on the effect of *Fr* and Re on the transition between the weakly stratified turbulence to the strongly stratified turbulence regimes. Moreover, Pal et al. (2017) used direct numerical simulations (DNS) in physical space to study the transition from near wakes to stratified turbulent wakes. The previous studies mainly concentrated on internal lee waves or non-stationary wake structures. To further elucidate the evolution mechanism of internal wave wakes, it is necessary to conduct a systematic study.

The present study focuses on the influences of hydrodynamic parameters on the large-scale internal wave wake signatures in the pycnocline and turbulence characteristics in the wakes of a submerged body based on numerical simulations. Section 2 introduces the numerical algorithm and setups used in this paper. The analyses of internal wave wakes, including internal lee waves and turbulent wakes, are presented in Sec. 3. Finally, a conclusion is given in Sec. 4.

2. Formulation of problem

2.1. Governing equations and numerical method

Internal wave wakes generated by a moving submerged body are obtained by solving the Navier-Stokes equations under the Boussinesq approximation:

$$\nabla \cdot \boldsymbol{u} = 0, \tag{1}$$

$$\frac{\partial \rho_w \boldsymbol{u}}{\partial t} + \nabla \cdot (\rho_w \boldsymbol{u}\boldsymbol{u}) = -\nabla p + \nabla \cdot (2\mu \boldsymbol{S}) + (\rho_w + \rho_{s0} + \rho_d)\boldsymbol{g}, \tag{2}$$

where $\nabla = (\partial/\partial x, \partial/\partial y, \partial/\partial z)$ is the gradient operator, $\boldsymbol{u}$ the velocity vector, p the pressure, μ the dynamic viscosity coefficient, $\boldsymbol{S} = (\nabla \boldsymbol{u} + \nabla \boldsymbol{u}^T)/2$ the strain-rate tensor, and $\boldsymbol{g} = (0, -g, 0)$ the acceleration due to gravity. The total density can be divided into three parts, namely

$$\rho = \rho_w + \rho_{s0} + \rho_d. \tag{3}$$

ρ_w is the uniform part of the background density, which is chosen as the density of water on the ocean surface, *i.e.* $\rho_w = \rho(\varphi = 0)$. Here, φ is the depth defined as $\varphi = y_{surface} - y$, where $y_{surface}$ is the vertical coordinate of the top boundary. ρ_{s0} represents the stable stratification and ρ_d is the disturbance. ρ_d can be solved with the density transport equation

$$\frac{\partial \rho_d}{\partial t} + \nabla \cdot ((\rho_{s0} + \rho_d)\boldsymbol{u}) = \nabla \cdot D \nabla (\rho_{s0} + \rho_d), \tag{4}$$

where ρ_{s0} is supposed to be time-invariant and D is the diffusion coefficient. We use an in-house code described in Yang et al. (2021) for the fundamental fluid dynamics solution. Decomposition of density stratification and solution of density transport equation are newly implemented and added into the main program to simulate the density fluctuation.

A summary of the numerical methodology is provided here, and a more detailed description of space discretization and time stepping can refer to Yang et al. (2021). The governing equations are solved numerically on staggered Cartesian grids, where vector quantities are defined on the cell faces, and scalar quantities are stored at the cell centers. The grids are refined locally in the streamwise and spanwise directions in the region that contains the submerged body, and uniform grids are used in the vertical direction with fine resolution. The resolution of the grid is chosen with the convergence of main features investigated of internal wave wakes. A second-order Runge-Kutta (RK2) method is used for time stepping for both the momentum equation (2) and the additional density transport equation (4). Under the Boussinesq approximation, in each substep of the RK2 algorithm, the fractional step method is applied to satisfy the divergence-free condition given by Eq. (1). The derivatives are calculated with a finite-difference scheme. The linear interpolation and the third-order CUI interpolation scheme are used for the advection terms to assure simulation convergence, while the other terms are interpolated linearly. We remark that the same numerical scheme and interpolation techniques are used for the density equation to keep consistency. In particular, CUI interpolation stands for *Cubic Upwind Interpolation* and is a total variation diminishing and convection-boundedness criterion satisfying convective limiter. For an arbitrary quantity χ, the CUI scheme requires three stencil points located respectively far upwind (designated with subscript u), upwind (designated with subscript c), and downwind (designated with subscript d). The interpolation process is expressed as

$$\tilde{\chi} = \chi_u + \hat{\tilde{\chi}}(\chi_d - \chi_u),$$

$$\hat{\tilde{\chi}} = \begin{cases} 3\hat{\chi}_c, & 0 < \hat{\chi}_c \le \frac{2}{13}, \\ \frac{5}{6}\hat{\chi}_c + \frac{1}{3}, & \frac{2}{13} < \hat{\chi}_c \le \frac{4}{5}, \\ 1, & \frac{4}{5} < \hat{\chi}_c \le 1, \\ \hat{\chi}_c, & \hat{\chi}_c \le 0 \text{ or } \hat{\chi}_c > 1, \end{cases} \tag{5}$$

$$\hat{\chi}_c = \frac{\chi_c - \chi_u}{\chi_d - \chi_u}.$$

The large eddy simulation is applied to filter the governing equations, and the VREMAN model is chosen as the subgrid-scale eddy viscosity model. Further details about this subgrid model can refer to Vreman (2004) and Ghaisas et al. (2013).

2.2. Simulation setup and cases

A schematic of the simulation setup is shown in Fig. 1. There are two different computational domains of respective sizes, $L_x \times L_y \times L_z = 60d \times 30d \times 50d$ and $L_x \times L_y \times L_z = 100d \times 30d \times 50d$, where d is the diameter of the body. The density variation in the pycnocline is continuous, and the density difference between the top and bottom of the pycnocline is constant so that with the increase of the pycnocline thickness Δ_L, the corresponding buoyancy frequency decreases. The density stratification with a hyperbolic tangent profile can be expressed as

$$\rho(y) = \overline{\rho} - \Delta\rho \tanh\left(\frac{y - y_{pyc}}{\Delta_L}\right), \tag{6}$$

where $\overline{\rho}$ is the fixed average value of the density and y_{pyc} is the center position of the pycnocline. An example of the density profile for $\Delta_L/d = 1$, together with the corresponding buoyancy frequency profile calculated by $N(y) = \sqrt{-g\frac{\partial \ln \rho}{\partial y}}$, is given in Fig. 2.

The submerged body without appendage is captured by the immersed boundary (IB) method. In the spanwise direction, a periodic condition is applied for all variables. A free slip boundary condition for velocity is applied to both top and bottom boundaries to be consistent with in-outlet conditions in the streamwise direction. The inlet velocity profile is uniform while a convection condition is imposed at the outlet (see Fig. 1). For the density disturbance, a zero-gradient condition is applied for both inlet and outlet. We assume that the density disturbance satisfies the Dirichlet condition on top and bottom boundaries and apply the no-flux condition to the surface of the submerged body.

From geometrical parameter d and moving velocity U_0, four non-dimensional parameters are defined to investigate the influence of parameters on the internal wave wakes. They are the Froude number ($Fr = U_0/\sqrt{gd}$), the Reynolds number ($\mathrm{Re} = \rho_w U_0 d/\mu$), the relative position between the submerged body and the center of pycnocline Δ_d/d ($\Delta_d = y_{body} - y_{pyc}$ with y_{body} the position of the submerged body), and the thickness of pycnocline Δ_L/d (see Fig. 1). Table 1 displays the parameters used in various numerical experiments. Dimensional parameter $d = 15m$ is chosen for normalization according to the comparable order of actual submarine diameter, and the Froude numbers are calculated with $U_0 \in \{3, 4, \ldots 11\} \cup \{12.24\} m/s$.

3. Results and discussions

3.1. Quantitative measurements for internal Kelvin-wave patterns

In order to gain a quantitative understanding of internal lee waves, the wake angle, wavelength, and wave amplitude are extracted and analyzed. For free-surface Kelvin waves, the wake angle is identified by distinguishing the borderline between the transverse and divergent waves or by fitting the borderline through the highest peaks with the least square approximation (see Pethiyagoda et al., 2014). However, we concentrate on internal wave wakes near the pycnocline, which differ from free-surface Kelvin waves. The measurement method for wake angle is no longer suitable in our cases. As shown in Fig. 3(a), there are two types of components in the wakes: the large-scale stationary internal lee waves and the small-scale non-stationary waves. The wake angle can be identified by figuring out the border between these two types of waves. Then the angle can be quantified in three steps: *i)* find the peaks of wave amplitude on the cross-section; *ii)* find the border points of the region containing unsteady wakes; *iii)* calculate the slope of the borderline with the least square fitting and derive the angle. The border of unsteady wakes can be distinguished and verified by comparing wake peak locations at different instantaneous. In order to uniquely determine the wake angle, only points before the first intersection between points on the borderline and the stationary wake peaks are chosen for fitting. One example of measuring the wake angle is shown in Fig. 3(b).

Since internal lee waves are stationary, the wavelength and amplitude can be measured by extracting the wave profiles in the horizontal plane containing the pycnocline center. Two vertical cross-sections of the internal waves are displayed in Fig. 4. The vertical displacement of a wave is designated as Δ_y, representing the deformation of the isopycnal surface in the vicinity of a certain depth. From Fig. 4(b), it can be found that the wave profiles in the $x-y$ plane can be divided into two regions. One is a large-scale stationary wave with a longer wavelength corresponding to the internal lee waves. The other is a train of non-stationary waves with a much shorter carrier wavelength corresponding to the turbulent waves marked in Fig. 3(a). However, only longer-wavelength stationary waves exist in the z-cross-sections for $z \geqslant 5d$ (see Fig. 4(c) for $z = 5d$). In order to eliminate the effect of the non-stationary wave on the stationary one, the wavelength is featured by half in the z-cross-section at $z = 5d$, which is measured by the length between a crest and its adjacent trough, as shown in Fig. 4(c).

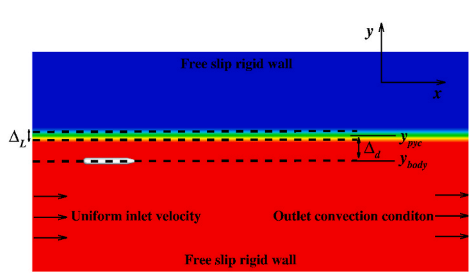

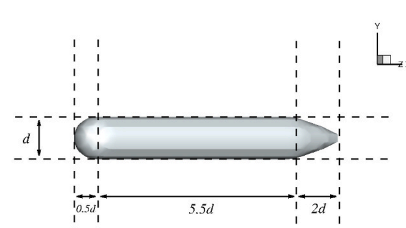

Fig. 1. Sketch of a submerged body in a stratified flow. The variation of background density is colored. (a) Illustration of the computational domain. (b) Geometry of the submerged body.

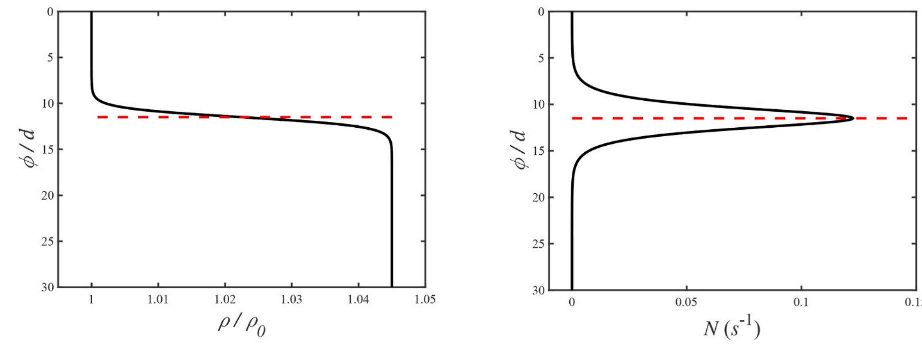

(a) (b)

Fig. 2. Schematic of density: (a) density profile of the stratified flow with the pycnocline thickness $\Delta_L = 1d$ (solid line); (b) the corresponding buoyancy frequency. The red dashed lines represent the pycnocline center. (For interpretation of the references to color in this figure legend, the reader is referred to the Web version of this article.)

Table 1
Parameters for various numerical experiments.

Fr	Δ_d/d	Δ_L/d	Re
0.4, 0.8, 1	−3.5, 0, 3.5	1	4×10^5
0.24, 0.33, 0.49, 0.57, 0.65, 0.73, 0.90	−3.5	1	4×10^5
0.4	−3.5, −4.5, −5.5	1	4×10^5
0.4	−3.5	1, 2, 4	4×10^5
0.4	−3.5	0.5, 1.5, 2.5, 3, 3.5	4×10^5
0.4	−3.5	1	4×10^5, 4×10^4, 4×10^3

3.2. *Characteristics of internal lee waves*

3.2.1. *Influence of the position of submerged body on internal lee waves*

To illuminate the influence of the submerged body position on the internal waves, we place the body at three different positions, namely below the pycnocline ($\Delta_d/d = -3.5$), at the center of the pycnocline ($\Delta_d/d = 0$), and above the pycnocline ($\Delta_d/d = 3.5$), respectively. Wave fields at a depth of the pycnocline center and wave profiles for the vertical cross-sections at $z = 0$ and $z = 5d$ are displayed in Figs. 5 and 6, respectively. For the cases of $\Delta_d/d = -3.5$ and $\Delta_d/d = 3.5$, it can be seen that the patterns of internal lee waves are similar (see Fig. 5(a) and (c)). The wake angles are 16.70° and 16.54°, with a relative difference of less than 1%, as shown in Fig. 5. It is shown in Fig. 6 that the wavelength and wave amplitude are almost the same. The difference between these two cases is revealed by the opposite locations of the crest and trough. Figs. 5 (a) and 6(a) also indicate that there are non-stationary turbulent waves with a higher intensity close to the centerline when the submerged body is located below the pycnocline, while in Fig. 5(c), the non-stationary components are less evident. That is because the buoyancy effect drives the wave propagation upwards to the pycnocline. When the submerged body is located at the center of the pycnocline (see Fig. 5(b)), the wake angle of the internal lee waves is reduced to 9.09°. The wave pattern becomes more complicated due to the interaction between the internal lee waves and the non-stationary turbulent waves right after the submerged body. In this case, the cross-section profiles in the $x - y$ plane (see Fig. 6(a)) show that the wave amplitude is the largest among the three, but the wavelength is relatively shorter (see Fig. 6(b)).

As the buoyancy effect on the internal wave patterns is apparent when the submerged body is located below the pycnocline, the internal wave wakes generated by submerged body at different depths below the pycnocline are investigated. From Figs. 7 and 8, it can be observed that the internal wave patterns are the same. By increasing the depth, the value of wake angle increases, namely 16.70°, 17.48°, and 19.39°, respectively. The variation of wavelength is relatively small for these cases. However, the wave amplitude decreases significantly due to the dissipation during the vertical upwards propagation. A sound conclusion that the diving depth of the submerged body mainly affects the amplitude of internal waves is then obtained.

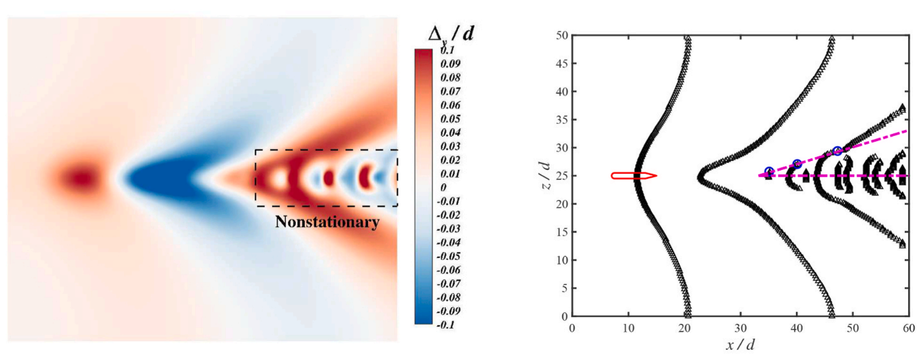

(a) (b)

Fig. 3. Example of measuring the wake angle of an internal lee waves in the pycnocline. Numerical parameters are $Fr = 0.4$, $\Delta_d/d = -3.5$, and $\Delta_L/d = 1$. (a) Wave field at $y = 18.5d$, where the pycnocline center is located. The region that contains non-stationary wakes is marked. (b) Peaks of wave amplitude (triangle) and the borderline interpolated (circle and pink dashed line). The simplified geometry of the submerged body is also presented (red solid line). The slope of borderline is $s = 0.30$, and the wake angle is derived as $\arctan s \cdot 180/\pi = 16.70°$. (For interpretation of the references to color in this figure legend, the reader is referred to the Web version of this article.)

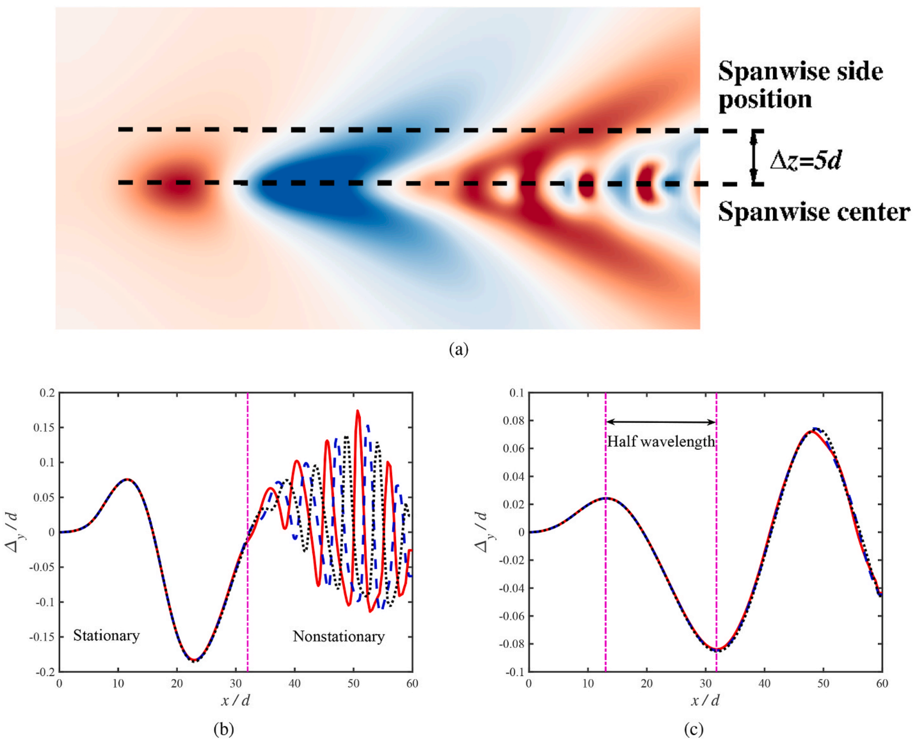

Fig. 4. Cross-sections of the generated internal waves with $Fr = 0.4$, $\Delta_d/d = -3.5$, and $\Delta_L/d = 1$. (a) Schematic of two positions: $z = 0$ and $z = 5d$. (b) Wave profiles in the $x - y$ plane. (c) Wave profiles in the plane $z = 5d$. Different line styles represent the wave profiles at different instantaneous $T = 96d/U_0$ (red solid), $98d/U_0$ (blue dashed), and $100d/U_0$ (black dotted). (For interpretation of the references to color in this figure legend, the reader is referred to the Web version of this article.)

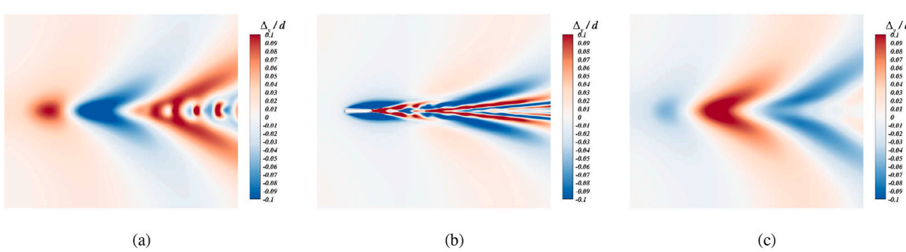

Fig. 5. Wave fields at a depth of the pycnocline center ($y/d = 18.5$) with $\Delta_L/d = 1$ and $Fr = 0.4$ for the submerged body placed at three different levels: (a) below the pycnocline $\Delta_d/d = -3.5$; (b) at the center of the pycnocline $\Delta_d/d = 0$; (c) above the pycnocline $\Delta_d/d = 3.5$.

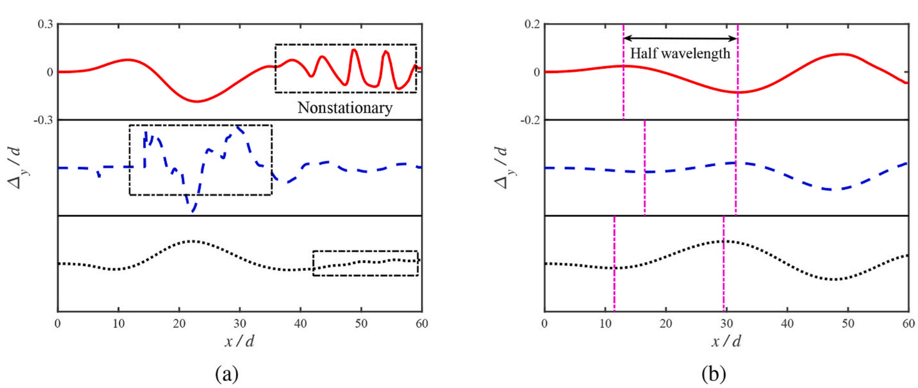

Fig. 6. Comparisons of z-cross-sections of the internal waves generated by a submerged body at different positions: $\Delta_d/d = -3.5$ (solid red), $\Delta_d/d = 0$ (dashed blue), and $\Delta_d/d = 3.5$ (dotted black), and other parameters are $\Delta_L/d = 1$ and $Fr = 0.4$. (a) The cross-sections in the $x - y$ plane, with the unsteady regions highlighted. (b) The cross-sections in the vertical plane $z = 5d$. (For interpretation of the references to color in this figure legend, the reader is referred to the Web version of this article.)

3.2.2. *Influence of the Reynolds number on internal lee waves*

Previous studies usually established inviscid theoretical models for internal waves (Keller and Munk, 1970; Darmon et al., 2014). To understand the viscous effect on internal wave wakes, we keep the velocity and length scales but change the kinematic viscosity coefficient or, equivalently, the Reynolds number Re. The field plots and cross-sections of the internal waves obtained with the parameters $\Delta_d/d = -3.5$, $\Delta_L/d = 1$, $Fr = 0.4$, and different Reynolds numbers are displayed in Figs. 9 and 10. The internal waves exhibit a similar structure. For internal lee waves, the increase of Re leads to a slight decrease in wake angle,

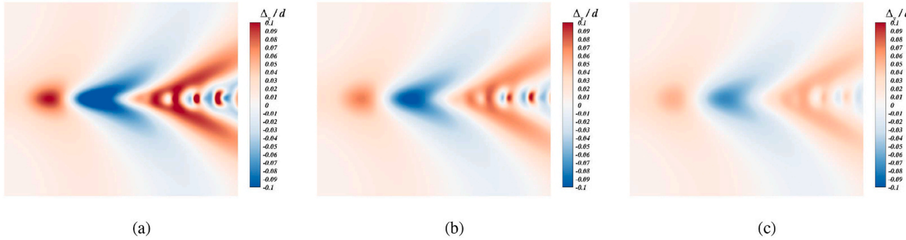

Fig. 7. Wave fields at a depth of the pycnocline center ($y/d = 18.5$) with $\Delta_L/d = 1$ and $Fr = 0.4$ for a submerged body placed at three different depths: (a) $\Delta_d/d = -3.5$; (b) $\Delta_d/d = -4.5$; (c) $\Delta_d/d = -5.5$.

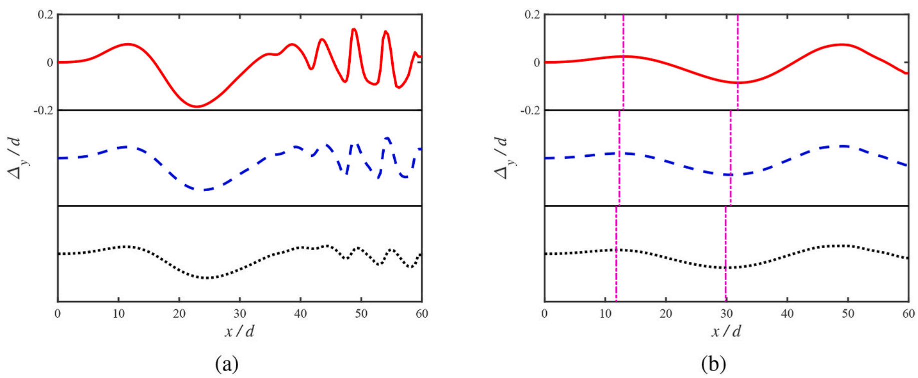

Fig. 8. Comparisons of wave amplitude and wavelength for the internal waves generated by a submerged body placed at three different depths below the pycnocline: $\Delta_d/d = -3.5$ (solid red), $\Delta_d/d = -4.5$ (dashed blue), and $\Delta_d/d = -5.5$ (dotted black), and other parameters are $\Delta_L/d = 1$ and $Fr = 0.4$. (a) The cross-sections in the $x - y$ plane. (b) The cross-sections in the vertical plane $z = 5d$. (For interpretation of the references to color in this figure legend, the reader is referred to the Web version of this article.)

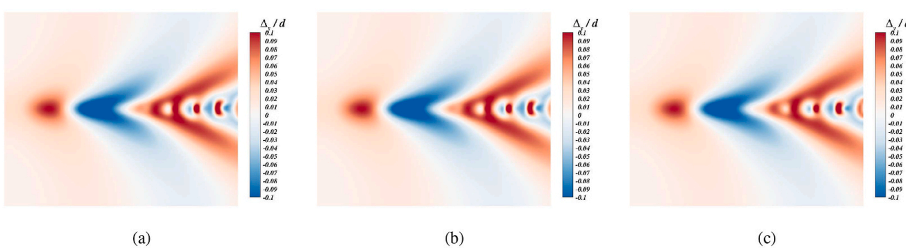

Fig. 9. Wave fields at a depth of the pycnocline center ($y/d = 18.5$) with $\Delta_d/d = -3.5$, $\Delta_L/d = 1$, $Fr = 0.4$, and different Reynolds numbers: (a) Re $= 4 \times 10^5$; (b) Re $= 4 \times 10^4$; (c) Re $= 4 \times 10^3$.

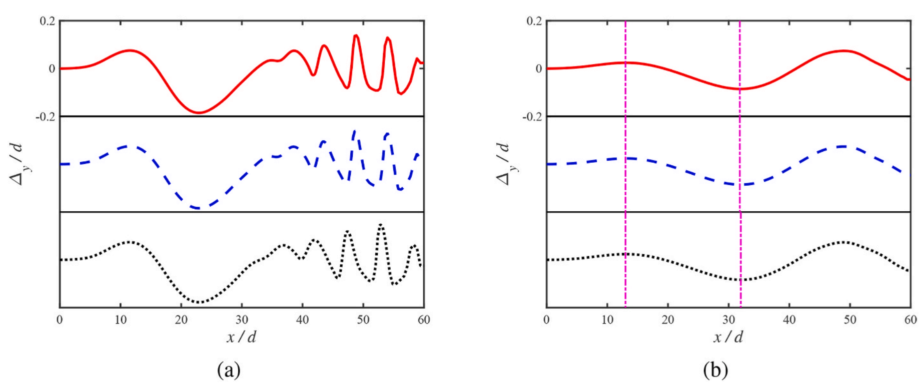

Fig. 10. Comparisons of wave amplitude and wavelength for the internal waves obtained with $\Delta_d/d = -3.5$, $\Delta_L/d = 1$, $Fr = 0.4$, and different Reynolds numbers: Re $= 4 \times 10^5$ (solid red), Re $= 4 \times 10^4$ (dashed blue), and Re $= 4 \times 10^3$ (dotted black). (a) The cross-sections in the $x - y$ plane. (b) The cross-sections in the vertical plane $z = 5d$. (For interpretation of the references to color in this figure legend, the reader is referred to the Web version of this article.)

namely 16.70°, 16.49°, and 16.12°, respectively. And the relative variations of wavelength and wave amplitude are only about 1%. It indicates that the viscosity seems to have little effect on internal lee waves within a certain range.

3.2.3. *Influence of the pycnocline thickness on internal lee waves*

The density of seawater varies with temperature and salinity. A stable density stratification exists in the form of the pycnocline. To appreciate the influence of changing the pycnocline thickness Δ_L/d on internal wave wakes, we show in Fig. 11 the corresponding wave fields

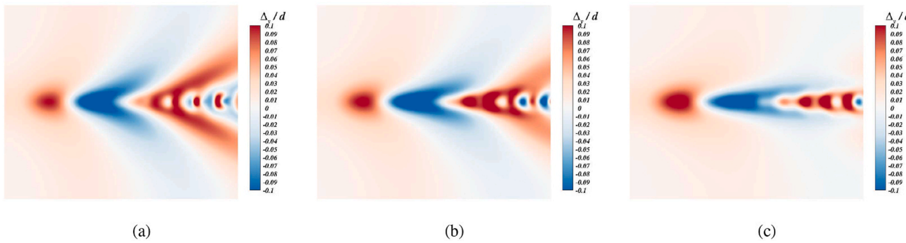

Fig. 11. Wave fields at a depth of the pycnocline center ($y/d = 18.5$) with $\Delta_d/d = -3.5$, $Fr = 0.4$, and different pycnocline thicknesses: (a) $\Delta_L/d = 1$; (b) $\Delta_L/d = 2$; (c) $\Delta_L/d = 4$.

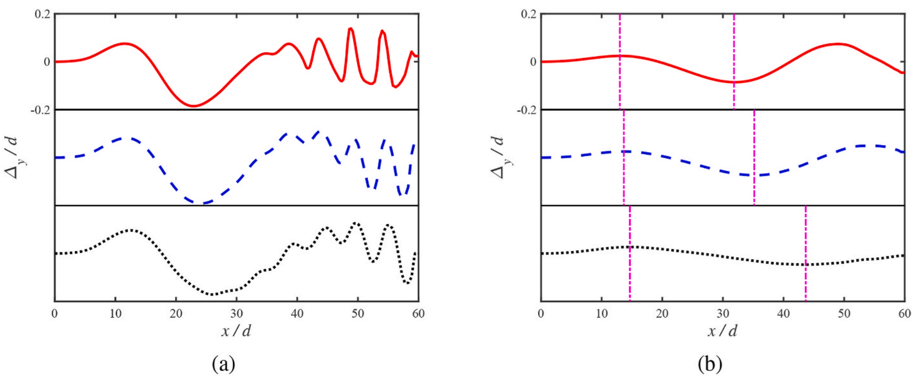

Fig. 12. Comparison of wave amplitude and wavelength for the internal waves obtained with $\Delta_d/d = -3.5$, $Fr = 0.4$, and different pycnocline thicknesses: $\Delta_L/d = 1$ (solid red), $\Delta_L/d = 2$ (dashed blue), and $\Delta_L/d = 4$ (dotted black). (a) The cross-sections in the $x - y$ plane. (b) The cross-sections in the vertical plane $z = 5d$. (For interpretation of the references to color in this figure legend, the reader is referred to the Web version of this article.)

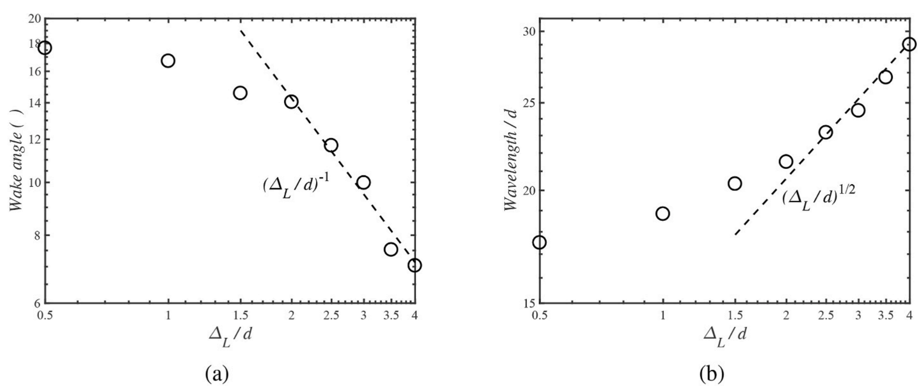

Fig. 13. Wake angle and wavelength of internal lee waves as a function of Δ_L/d. The logarithmic view is used for the presentation of scalings. (a) Wake angle. (b) Wavelength.

with the same diving depth and moving velocity of the submerged body. By comparing the internal wave fields, it is clear that with the increase of the pycnocline thickness, there are reductions in wake angle and wave amplitude, but the wavelength increases. This fact can be quantified by the cross-sections in the vertical plane $z = 5d$ in Fig. 12(b).

For further quantitative analyses, more numerical cases were performed. The wake angle and wavelength are plotted as a function of Δ_L/d in Fig. 13. The wake angle decreases slowly for relatively small pycnocline thicknesses ($\Delta_L/d < 1.5$). Then it significantly reduces and follows a scaling as $(\Delta_L/d)^{-1}$ (for $\Delta_L/d > 2$). We remark that the power laws are found in the logarithm view, so the power function has a linear presentation. In contrast, the wavelength is markedly on the rise and

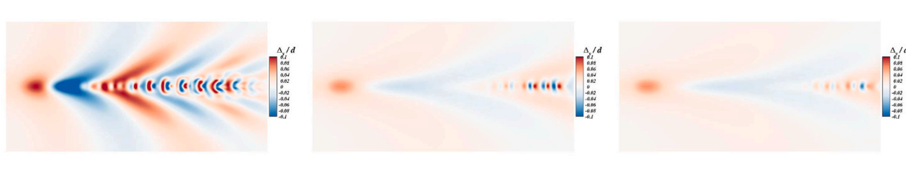

Fig. 14. Wave fields at a depth of the pycnocline center ($y/d = 18.5$) with $\Delta_d/d = -3.5$, $\Delta_L/d = 1$, and different Froude numbers: (a) $Fr = 0.4$; (b)$Fr = 0.8$; (c)$Fr = 1$. The wake angles are 16.70°, 8.53°, and 6.28° from (a) to (c), respectively.

seems to follow a scaling as $(\Delta_L/d)^{1/2}$ for $\Delta_L/d > 2$.

3.2.4. Influence of the Froude number on internal lee waves

In this part, the influence of the Froude number on internal waves is investigated by varying the moving velocity. The domain size $L_x \times L_y \times L_z = 100d \times 30d \times 50d$ is applied to capture the information in the far field for high Froude numbers ($Fr > 0.6$). As seen from the wave fields shown in Fig. 14, by increasing the Froude number, the internal lee waves extend far downstream, and the wake angle significantly decreases. The cross-sections of waves in Fig. 15 indicate that the wavelength increases significantly and the wave amplitude decreases, along with the increase of *Fr*. For small-scale turbulent wakes, the internal lee waves play an essential role in interacting with them and changing their behaviors (see the case of $Fr = 0.4$). At higher moving velocities, the effect of internal lee waves becomes weaker, and the occurrence of non-stationary turbulent wake moves downstream.

More numerical experiments have been conducted to determine the wake angle and wavelength as functions of *Fr*. The wake angles of internal lee waves are measured and plotted in Fig. 16(a). It shows that the scaling of the decrease of wake angle is Fr^{-1}. In Fig. 16(b), the wavelength presents a linear variation with *Fr*. The tendency is in agreement with the measurements by Meunier et al. (2018).

3.3. The summary of variation trend for the internal lee waves

The above analyses offer a preliminary understanding of the effects of hydrodynamic parameters on internal lee waves. To present the results more intuitively, we draw a trend diagram in Fig. 17 to illustrate the dependence of the observed internal lee waves' features on hydrodynamic parameters. The trend diagram shows only the results of representative numerical experiments, not all the cases. For example, three magenta-triangle marks represent three typical cases with different pycnocline thicknesses. In particular, three cases with various Froude numbers for three relative positions between the submerged body and pycnocline (above, in the center, and below), in a total of nine circle marks (red, blue, and black), are shown in the diagram. The variation tendency is described by the dotted lines with arrows. As shown in Fig. 17, it can be readily seen that the influence degree order is $Fr > \Delta_L > \Delta_d >$ Re. The order of influence can be analyzed by comparing rangeability. As the Reynolds number increases, wake angle and wave amplitude do not have noticeable change (green-star marks). By increasing the distance between the pycnocline and the submerged body below, wave amplitude decreases while wake angle slightly increases (cyan-square marks). Therefore, the effect of the Reynolds number and diving depth is minor. The moving velocity (*Fr*) and the density stratification (Δ_L/d) are two key parameters for internal lee waves. The increase of *Fr* leads to the reduction of both wake angle and wavelength (circle marks). The density stratification (Δ_L/d) has the same influence trend as *Fr* (magenta-triangle marks). From Fig. 17, the order of influence, $Fr > \Delta_L/d$, can be obtained by comparing the variation of wake angle and wave amplitude when two parameters increase with the same multiplier factor (say, 2). Moreover, considering the power laws in Figs. 13(b) and 16(b), the order of scaling in the function of *Fr* is higher than the one of Δ_L/d, which also confirms the conclusion on the order of influence. In addition, when the submerged body is located at different depths, the variation trend of wake angle and wavelength with *Fr* is the same. However, the wake angle and wavelength values for a submerged body placed at the pycnocline center differ from those located below or above.

3.4. The characteristics of turbulent wakes in a stratified flow

To gain insight into stratification effects on the vortex structures in the wake, the instantaneous iso-surfaces of Q-criterion ($Q = 0.005$), colored by the spanwise vorticity ω_z at the cases with and without density stratification, are displayed in Fig. 18. In both cases, organized vortices appear and move upwards in the wake near the submerged body. We can observe the generation and shedding of hairpin vortices from the tail of the submerged body, which is coherent with results in Qu et al. (2021) with higher resolution in wake vortex region. However, vertical motions of vortices in the stratified flow are suppressed, and vortices break up into small-scale ones downstream due to the existence of the pycnocline.

Fig. 19 exhibits the distributions of turbulent kinetic energy in the $x - y$ plane to investigate further the influence of density stratification on the turbulent wake. Turbulent kinetic energy is calculated by over 60 instantaneous velocity fields. The fields of turbulent kinetic energy can be separated into two regions, one is the near wake, and the other is the far wake. In the near wake, the distributions are almost similar in both cases. The concentration of turbulent kinetic energy in the near wake develops vertically, and the rangeability in the homogeneous case is slightly wider than in the stratified flow, similar to the observation in Huang et al. (2022) for $x/d \leqslant 10$. In the far wake, the distribution changes, and the intensity of turbulent kinetic energy in stratified flow becomes weaker than in the homogeneous flow. It further indicates that density stratification plays a role in weakening turbulent kinetic energy.

To understand the vertical propagation process of turbulent kinetic energy, we plot in Fig. 20 the distributions at different depths ($y/d = 18$, 18.5, 19, 20). In the stratified flow, the turbulent wakes are similar to the Kelvin-wake pattern but oscillate with a shorter wavelength. These observations demonstrate that the turbulent wakes are modulated by internal lee waves, as mentioned in Pal et al. (2017). On the contrary, in the homogeneous flow, the turbulent wakes maintain approximately circular structures, and the distance between two successive structures is more significant than in the stratified case. With the increment of the

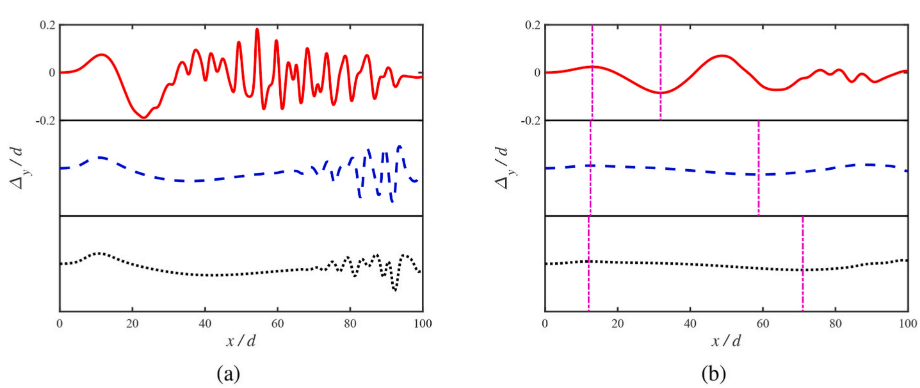

Fig. 15. Comparisons of wave amplitude and wavelength for the internal waves obtained with $\Delta_d/d = -3.5$, $\Delta_L/d = 1$, and different Froude number: $Fr = 0.4$ (solid red), $Fr = 0.8$ (dashed blue), and $Fr = 1$ (dotted black). (a) The cross-sections in the $x - y$ plane. (b) The cross-sections in the vertical plane $z = 5d$. (For interpretation of the references to color in this figure legend, the reader is referred to the Web version of this article.)

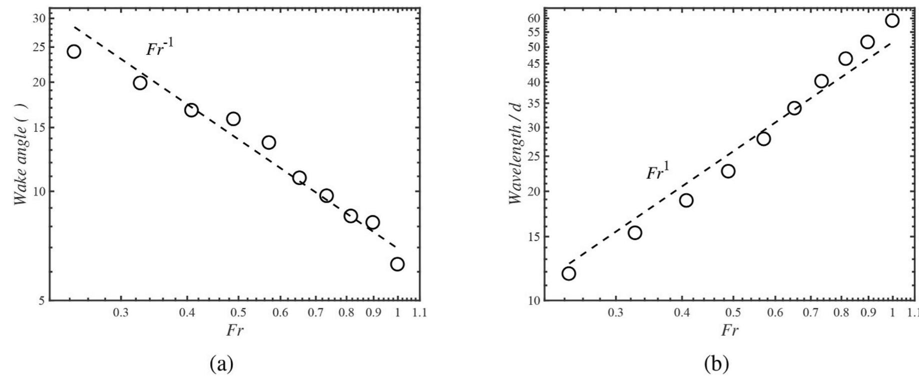

Fig. 16. Scaling characteristics of the Kelvin-wave pattern as a function of the Froude number, where the logarithmic view is used. (a) Wake angle. (b) Wavelength.

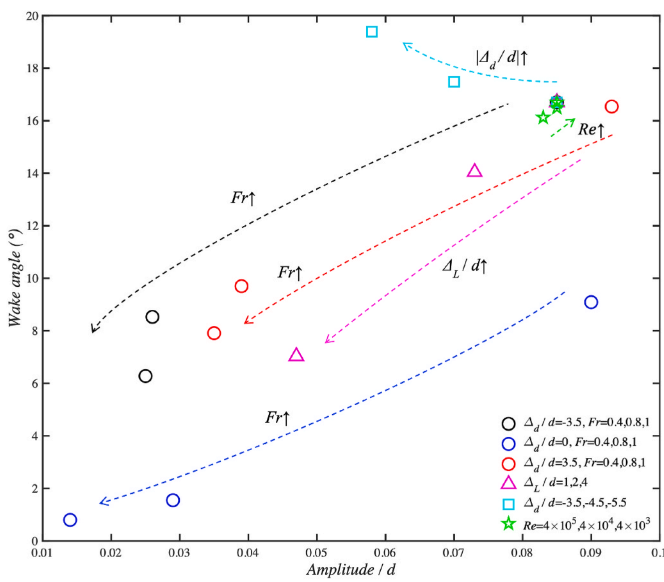

Fig. 17. Scattergram (wave amplitude versus wake angle) of the results with different sets of parameters.

vertical position (y/d), turbulent kinetic energy decreases and gradually concentrates on the far wake in both cases and the vertical positions that the turbulent kinetic energy can reach in both cases are similar ($y/d \leqslant 21$). Nevertheless, a more concentrated distribution of turbulent kinetic energy with higher intensity is shown in the homogeneous case. The difference in turbulence intensity shows that the presence of pycnocline hampers the vertical propagation or the penetration of the pycnocline. This observation can be analogous to the propagation of internal waves in stratified flow with the presence of a pycnocline. Namely, with a sudden increase in buoyancy frequency, the angle between the vertical direction and the propagation direction increases dramatically, which means the vertical propagation is weakened.

4. Conclusions

A series of numerical simulations have been conducted to explore the effects of hydrodynamic parameters on internal wave wakes. The primary findings are listed as follows.

1. A measure method of wake angles of internal lee waves, based on distinguishing the border between stationary lee waves and non-stationary turbulent waves, is proposed.
2. The influences of hydrodynamic parameters on internal lee waves are summarized in a trend diagram. Four parameters for the internal lee waves, the influence degree in order is the Froude number, the pycnocline thickness, the submerge body position, and the Reynold number. Both the Froude number (the moving velocity) and the pycnocline thickness play an important role in the characteristics of the internal lee waves. The wake angle decreases as Fr^{-1} and wavelength presents a linear variation with Fr.
3. The effects of density stratification on turbulent wakes are investigated. It reveals that the density stratification changes the wake structures due to the existence of the internal lee waves and has a weakening effect on turbulent kinetic energy.

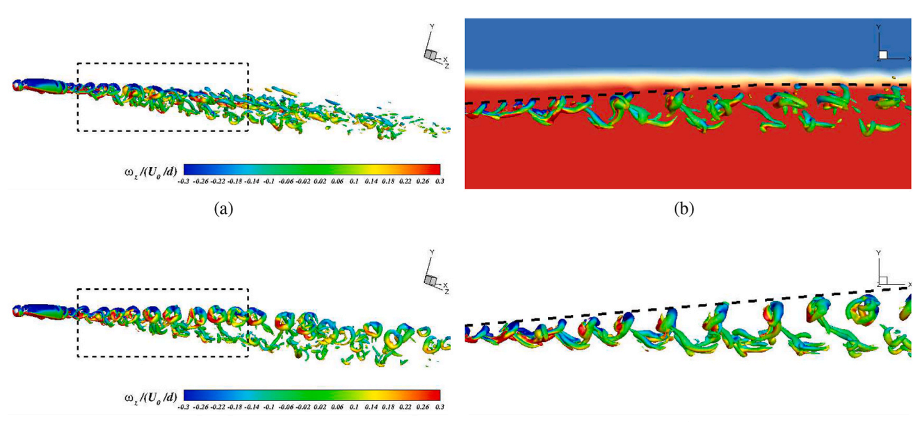

Fig. 18. Isosurfaces of Q level, colored by the spanwise component of vorticity ω_z. (a) Results for a stratified flow. (b) Zoom in view with a density stratification ($x - y$ view). (c) Results for a homogeneous flow. (d) Zoom in view ($x - y$ view).

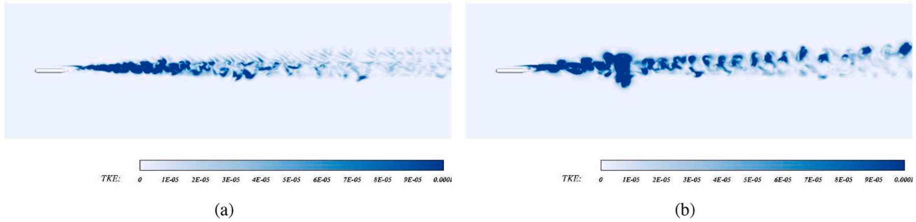

Fig. 19. Comparison of turbulent kinetic energy in the $x-y$ section. (a) Results for a stratified flow. (b) Results for a homogeneous flow.

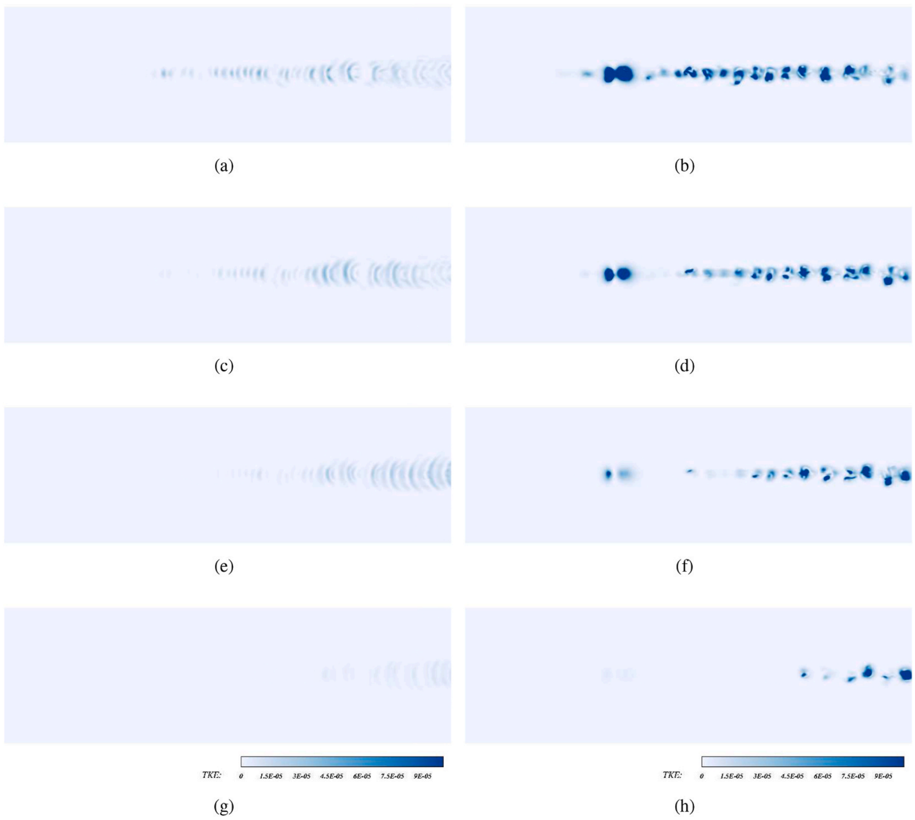

Fig. 20. Comparisons of turbulent kinetic energy in different horizontal planes: $y/d=18$, $y/d=18.5$, $y/d=19$, and $y/d=20$, respectively, from top to bottom. Left: results for a stratified flow, where the center of the pycnocline is at $y/d=18.5$. Right: results for a homogeneous flow.

CRediT authorship contribution statement

Jin Chai: Methodology, Software, Visualization, Data curation, Writing – original draft. **Zhiying Wang:** Methodology, Supervision, Validation, Writing – review & editing. **Zixuan Yang:** Methodology, Supervision. **Zhan Wang:** Conceptualization, Methodology, Supervision, Writing – review & editing.

Declaration of competing interest

The authors declare that they have no known competing financial interests or personal relationships that could have appeared to influence the work reported in this paper.

Data availability

No data was used for the research described in the article.

Acknowledgement

This work was supported by Key Program of the National Natural Science Foundation of China (No. 12132018) and Project of INTERNATIONAL COOPERATION and Exchanges NSFC (No. 11911530171).

References

Abdilghanie, A., Diamessis, P.J., 2013. The internal gravity wave field emitted by a stably stratified turbulent wake. J. Fluid Mech. 720, 104–139. https://doi.org/10.1017/jfm.2012.640.

Ali, L., Bai, Y., Xu, Y., 2022. A methodology to derive design metocean internal wave current criteria for submarine structures. Ships Offshore Struct. 17 (2), 388–397. https://doi.org/10.1080/17445302.2020.1834268.

Bonneton, P., Chomaz, J.M., Hopfinger, E.J., 1993. Internal waves produced by the turbulent wake of a sphere moving horizontally in a stratified fluid. J. Fluid Mech. 254, 23–40. https://doi.org/10.1017/S0022112093002010.

Bonnier, M., Eiff, O., 2002. Experimental investigation of the collapse of a turbulent wake in a stably stratified fluid. Phys. Fluids 14 (2), 791–801. https://doi.org/10.1063/1.1429963.

Borovikov, V.A., Bulatov, V.V., Vladimirov, Y.V., 1995. Internal gravity waves excited by a body moving in a stratified fluid. Fluid Dynam. Res. 15 (5), 325–336. https://doi.org/10.1016/0169-5983(94)00050-A.

Brandt, A., Rottier, J., 2015. The internal wavefield generated by a towed sphere at low froude number. J. Fluid Mech. 769, 103–129. https://doi.org/10.1017/jfm.2015.96.

Chen, Q., Lin, Q., Xuan, Y., Han, Y., 2021. Investigation on the thermohaline structure of the stratified wake generated by a propagating submarine. Int. J. Heat Mass Tran. 166, 120808 https://doi.org/10.1016/j.ijheatmasstransfer.2020.120808.

Darmon, A., Benzaquen, M., Raphaël, E., 2014. Kelvin wake pattern at large froude numbers. J. Fluid Mech. 738, R3. https://doi.org/10.1017/jfm.2013.607.
Dias, F., 2014. Ship waves and kelvin. J. Fluid Mech. 746, 1–4. https://doi.org/10.1017/jfm.2014.69.
Ding, W., Ai, C., Jin, S., Lin, J., 2020. 3d numerical investigation of forces and flow field around the semi-submersible platform in an internal solitary wave. Water 12 (1). https://doi.org/10.3390/w12010208.
Ghaisas, N.S., Shetty, D.A., Frankel, S.H., 2013. Large eddy simulation of thermal driven cavity: evaluation of sub-grid scale models and flow physics. Int. J. Heat Mass Tran. 56 (1), 606–624. https://doi.org/10.1016/j.ijheatmasstransfer.2012.09.055.
Gray, E.P., Hart, R.W., Farrell, R.A., 1983. The structure of the internal wave mach front generated by a point source moving in a stratified fluid. Phys. Fluids 26 (10), 2919–2931. https://doi.org/10.1063/1.864057.
Guo, L., Duan, M., Zhu, Z., 2022. A dynamic model of deep water riser and its global response characteristics induced by ocean internal wave and floating platform. Ships Offshore Struct. 17 (7), 1592–1603. https://doi.org/10.1080/17445302.2021.1937793.
Hartharn-Evans, S.G., Carr, M., Stastna, M., Davies, P.A., 2022. Stratification effects on shoaling internal solitary waves. J. Fluid Mech. 933, A19. https://doi.org/10.1017/jfm.2021.1049.
Huang, F., Meng, Q., Cao, L., Wan, D., 2022. Wakes and free surface signatures of a generic submarine in the homogeneous and linearly stratified fluid. Ocean Eng. 250, 111062 https://doi.org/10.1016/j.oceaneng.2022.111062.
Keller, J.B., Levy, D.M., Ahluwalia, D.S., 1981. Internal and surface wave production in a stratified fluid. Wave Motion 3 (3), 215–229. https://doi.org/10.1016/0165-2125(81)90015-9.
Keller, J.B., Munk, W.H., 1970. Internal wave wakes of a body moving in a stratified fluid. Phys. Fluids 13 (6), 1425–1431. https://doi.org/10.1063/1.1693096.
Lamb, K.G., Warn-Varnas, A., 2015. Two-dimensional numerical simulations of shoaling internal solitary waves at the asiaex site in the south China sea. Nonlinear Process Geophys. 22 (3), 289–312. https://doi.org/10.5194/npg-22-289-2015.
Ma, W., Li, Y., Ding, Y., Duan, F., Hu, K., 2020. Numerical investigation of internal wave and free surface wave induced by the darpa suboff moving in a strongly stratified fluid. Ships Offshore Struct. 15 (6), 587–604. https://doi.org/10.1080/17445302.2019.1661633.
Meunier, P., Le Dizès, S., Redekopp, L., Spedding, G.R., 2018. Internal waves generated by a stratified wake: experiment and theory. J. Fluid Mech. 846, 752–788. https://doi.org/10.1017/jfm.2018.278.
Meunier, P., Spedding, G.R., 2006. Stratified propelled wakes. J. Fluid Mech. 552, 229–256. https://doi.org/10.1017/S0022112006008676.
Pal, A., Sarkar, S., Posa, A., Balaras, E., 2017. Direct numerical simulation of stratified flow past a sphere at a subcritical Reynolds number of 3700 and moderate froude number. J. Fluid Mech. 826, 5–31. https://doi.org/10.1017/jfm.2017.398.
Pethiyagoda, R., McCue, S.W., Moroney, T.J., 2014. What is the apparent angle of a kelvin ship wave pattern? J. Fluid Mech. 758, 468–485. https://doi.org/10.1017/jfm.2014.530.
Pethiyagoda, R., McCue, S.W., Moroney, T.J., 2017. Spectrograms of ship wakes: identifying linear and nonlinear wave signals. J. Fluid Mech. 811, 189–209. https://doi.org/10.1017/jfm.2016.753.
Prasetya, I.A., Atmadipoera, A.S., Budhiman, S., Nugroho, U.C., 2021. Internal solitary waves in the northwest sumatra sea-Indonesia: from observation and modeling. IOP Conf. Ser. Earth Environ. Sci. 944 (1), 012056 https://doi.org/10.1088/1755-1315/944/1/012056.
Qiang, L., Boyer, D., Fernando, H., 1993. Internal waves generated by the turbulent wake of a sphere. Exp. Fluid 15 (2), 147–154. https://doi.org/10.1007/BF00190954.
Qu, Y., Wu, Q., Zhao, X., Huang, B., Fu, X., Wang, G., 2021. Numerical investigation of flow structures around the darpa suboff model. Ocean Eng. 239, 109866 https://doi.org/10.1016/j.oceaneng.2021.109866.
Rabaud, M., Moisy, F., 2013. Ship wakes: kelvin or mach angle? Phys. Rev. Lett. 110, 214503 https://doi.org/10.1103/PhysRevLett.110.214503.
Rabaud, M., Moisy, F., 2014. Narrow ship wakes and wave drag for planing hulls. Ocean Eng. 90, 34–38. https://doi.org/10.1016/j.oceaneng.2014.06.039.
Robey, H.F., 1997. The generation of internal waves by a towed sphere and its wake in a thermocline. Phys. Fluids 9 (11), 3353–3367. https://doi.org/10.1063/1.869448.
Spedding, G.R., 1997. The evolution of initially turbulent bluff-body wakes at high internal froude number. J. Fluid Mech. 337, 283–301. https://doi.org/10.1017/S0022112096004557.
Spedding, G.R., 2014. Wake signature detection. Annu. Rev. Fluid Mech. 46 (1), 273–302. https://doi.org/10.1146/annurev-fluid-011212-140747.
Stastna, M., Coutino, A., Walter, R.K., 2021. The effect of strong shear on internal solitary-like waves. Nonlinear Process Geophys. 28 (4), 585–598. https://doi.org/10.5194/npg-28-585-2021.
Vasholz, D., 2011. Stratified wakes, the high froude number approximation, and potential flow. Theor. Comput. Fluid Dynam. 25, 357–379. https://doi.org/10.1007/s00162-010-0207-5.
Voropayev, S.I., McEachern, G.B., Fernando, H.J.S., Boyer, D.L., 1999. Large vortex structures behind a maneuvering body in stratified fluids. Phys. Fluids 11 (6), 1682–1684. https://doi.org/10.1063/1.870030.
Vreman, A.W., 2004. An eddy-viscosity subgrid-scale model for turbulent shear flow: algebraic theory and applications. Phys. Fluids 16 (10), 3670–3681. https://doi.org/10.1063/1.1785131.
Wang, H., Chen, K., You, Y., 2017. An investigation on internal waves generated by towed models under a strong halocline. Phys. Fluids 29 (6), 693. https://doi.org/10.1063/1.4984988.
Wei, G., LE, J., Dai, S., 2003. Surface effects of internal wave generated by a moving source in a two-layer fluid of finite depth. Appl. Math. Mech. 24, 1025–1040. https://doi.org/10.1007/BF02437635.
Yang, Z., Lu, M., Wang, S., 2021. A robust solver for incompressible high-Reynolds-number two-fluid flows with high density contrast. J. Comput. Phys. 441, 110474 https://doi.org/10.1016/j.jcp.2021.110474.
Yeung, R.W., Nguyen, T., 1999. Waves generated by a moving source in a two-layer ocean of finite depth. J. Eng. Math. 35, 85–107. https://doi.org/10.1023/A:1004399917692.
Zhang, J., Yao, Z., Hong, F., Zhou, G., Gao, D., Su, B., 2021. On surface flow induced by internal waves generated by a slender body moving at low internal froude number in a sharply stratified fluid. Ocean Eng. 239, 109755 https://doi.org/10.1016/j.oceaneng.2021.109755.
Zhou, Q., Diamessis, P.J., 2019. Large-scale characteristics of stratified wake turbulence at varying Reynolds number. Phys. Rev. Fluid. 4, 084802 https://doi.org/10.1103/PhysRevFluids.4.084802.